Journal of Quantitative Spectroscopy & Radiative Transfer 110 (2009) 284–292

Contents lists available at ScienceDirect

Journal of Quantitative Spectroscopy & Radiative Transfer

journal homepage: www.elsevier.com/locate/jqsrt

Lifetime and transition probability determination in Xe IX

H.-P. Garnir [a,*], S. Enzonga Yoca [a,b], P. Quinet [a,c], É. Biémont [a,c]

[a] Institut de Physique Nucléaire, Atomique et Spectroscopie, Université de Liège, Sart Tilman B15, B-4000 Liège, Belgium
[b] CEPAMOQ, Faculty of Sciences, University of Douala, PO Box 8580 Douala, Cameroon
[c] Astrophysique et Spectroscopie, Université de Mons-Hainaut, B-7000 Mons, Belgium

ARTICLE INFO

Article history:
Received 28 October 2008
Accepted 16 November 2008

PACS:
32.70
31.15
41.75

Keywords:
Xe IX
Transition probabilities
Atomic lifetimes
Beam–foil

ABSTRACT

A new set of transition probabilities is proposed for Xe IX. They have been calculated by two different theoretical approaches i.e. a fully relativistic multiconfiguration Dirac–Fock (MCDF) method and a partly relativistic Hartree–Fock (HFR) approach taking core-polarization effects into account. Their accuracy has been evaluated through comparisons with lifetime measurements for 11 levels performed using beams of Xe^{+} ions produced by a 2 MV Van de Graaff accelerator. The agreement theory-experiment is nice for most of the levels and gives more weight to the theoretical models used for the calculations and, consequently, to the new transition probabilities.

1. Introduction

Investigating the atomic structure of the ions along the palladium isoelectronic sequence, and that of Xe IX in particular, is motivated by the progress realized in different fields of physics.

In astrophysics, the detection of collisionally excited transitions of xenon ions in the spectrum of the planetary nebula NGC 7027 has been discussed by Péquignot and Baluteau [1] and this was followed by calculations of collision strengths for electron impact excitation in selected xenon ions [2]. Abundances of s-process elements (including Kr and Xe) in planetary nebulae were also considered by Zhang et al. [3].

In plasma physics, a new class of short wavelength (XUV) lasers, in which an intense circularly polarized femtosecond pulse is used to ionize a gaseous target, has been developed [4]. As a specific application, a femtosecond-pulse driven 41.8-nm laser, based on the $4d^95d\,^1S_0-4d^95p\,^1P^0_1$ transition of Xe IX, has been developed by the same group [5]. It should be emphasized that Xe IX is a palladium-like system, analogous to the nickel-like ions, having a full subshell $4d^{10}$ ground state and excited configurations of the type $4d^9nl$ and that lasing occur on the $J=0$–1 5d−5p transitions.

Recently, EUV spectra of xenon ions have been recorded in the 4.5–20 nm wavelength region using an electron beam ion trap and a flat field spectrometer [6]. When varying the electron beam energy, the radiation emitted from the ions Xe^{6+} to Xe^{43+}, including thus Xe^{8+}, was observed.

The ground configuration of Xe IX is $4d^{10}$ and the first excited configurations are of the type $4d^9nl$ (with nl = 5s, 5p, 5d, 4f and 5f). In spite of this relative simplicity, our knowledge of the spectrum and of the radiative parameters of Xe IX is still very poor.

* Corresponding author. Tel.: +32 4366 3764; fax: +32 4366 28 84.
E-mail address: hpgarnir@ulg.ac.be (H.-P. Garnir).

0022-4073/$ - see front matter
doi:10.1016/j.jqsrt.2008.11.007

The resonance lines along the Pd I isoelectronic sequence have been investigated for the ions I VIII to Ho XXII [7]. The spectrum of Xe IX in the 40.0–120.0 nm wavelength range was studied by van Kampen et al. [8] by observing the radiation emitted following electron capture by Xe^{9+} and Xe^{8+} ion beams incident on a He gas target. All the levels of the $4d^95s$ and $4d^95p$ configurations have been established. The VUV spectra of the Pd-like ions from Xe IX through Ce XIII were analyzed and the $4d^95p-4d^95d$ and $4d^95d-4d^95f$ transitions were classified in Xe IX [9]. The uncertainty of their levels is about $20\,cm^{-1}$ with respect to the ground state and $5\,cm^{-1}$ relative to other levels. The spectra of various ions of xenon were investigated in the 7.0–17.0 nm region and the resonance transitions from the highly excited $4d^9(6p+5f+7p+6f)$ levels in Pd-like Xe IX were identified [10]. This led to five additional levels with uncertainties of about $20\,cm^{-1}$ for levels below $1\,100\,000\,cm^{-1}$ and more ($75\,cm^{-1}$) for higher levels. The most recent compilation on the energy levels and wavelengths of xenon ions was published by Saloman [11]. It is based on papers published up to 2004.

A few years ago, the spectral analysis of the $4d^95d$ and $4d^95f$ configurations of Xe IX was carried out on the basis of a spectrum in the 27.0–130.0 nm produced with a capillary light source [12]. This analysis was extended by Raineri et al. [13] to the $4d^96s$ configuration using spectra obtained by the same method in the region 27.0–200.0 nm. Some of these levels were, however, rejected in Saloman's [11] compilation.

Transition probabilities in the spectrum of Xe IX are also very scarce. The first work containing numerical data is probably due to Younger [14] who investigated the $4d^{10}\ ^1S-4d^94f\ ^1P^0$ resonance transition in the palladium isoelectronic sequence comparing three different approximations: configuration-averaged Hartree–Fock method, term-dependent Hartree–Fock approach and many-body perturbation theory. Transition probabilities for a few transitions of Xe IX were published by Churilov and Joshi [10], the main purpose of these authors being, however, the classification of the lines. Radiative lifetimes of the $4d^95p$ and $4d^95d$ levels in the ions Xe IX–Ce XIII were obtained by Loginov [15] using a semiempirical least-squares method for calculating the wavefunctions in intermediate coupling. Relativistic many-body perturbation theory (RMBPT), including the Breit interaction, was used to evaluate oscillator strengths and transition probabilities in Pd-like ions with nuclear charges Z ranging from 49 to 100 [16]. Finally, using a similar approach, wavelengths, transition rates, and line strengths have been calculated for multipole transitions between the excited $4p^64d^94f$, $4p^64d^95l$, $4p^54d^{10}4f$, and $4p^54d^{10}5l$ (l = s,p,d,f) configurations and the ground $4p^64d^{10}$ level in Pd-like ions with the nuclear charges ranging from $Z=47$ to 100 [17].

The present work is an extension of the analyses previously published by our group for neighboring xenon ions. In particular, transition probabilities have been calculated with the HFR + CP method for $\Delta n=0$ and 1 transitions connecting the $5s^25p^2$, $5s^25p6p$, $5s^25p4f$ and $5s5p^3$, $5s^25p5d$ and $5s^25p6s$ configurations of Xe V [18]. Using the same approach, we have investigated the $\Delta n=0$ and 1 transitions connecting the $5s^2nl$ [np, $n=5-8$; nf, $n=4-5$; nh, $n=6-8$], 5s5pnl (nl = 5d, 6s), $5p^3$ and $5s^2nl$ [ns, $n=6-8$; nd, $n=5-8$; ng, $n=5-6$; ni, $n=7-8$] and $5s5p^2$ configurations of Xe VI [19]. More recently, HFR + CP and MCDF lifetime values have been calculated in Xe VII and Xe VIII and compared to beam–foil measurements for 15 levels belonging to the configurations 5s5p, $5p^2$, 5s5d, 5s6s, 5p5d, 4f5p, 5p5d and 5s5f of Xe VII and 4 levels of the 5p and 5d configurations of Xe VIII [20].

In the present work, we propose a detailed set of transition probabilities for Xe IX transitions of interest for astrophysics and plasma physics. The accuracy of these new data is assessed through comparisons of theoretical lifetimes with experimental results obtained using the 2 MV Van de Graaff accelerator and the beam–foil device from Liège University.

2. Theoretical approaches

2.1. HFR calculations

In the present work, calculations of transition probabilities in Xe IX have been carried out firstly with the pseudo-relativistic Hartree–Fock (HFR) method [21] modified for taking core-polarization (CP) effects into account (see e.g. [22,23]) and called the HFR + CP method.

The following configurations were explicitly included in the physical model: $4d^{10}+4d^9ns\ (n=5-7)+4d^9nd\ (n=5-7)+4d^9ng\ (n=5-7)+4d^85s^2+4d^85p^2+4d^85d^2+4d^84f^2+4d^86s^2+4d^85s6s+4d^85snd\ (n=5-6)+4d^86s6d+4d^84f5p$ and $4d^9np\ (n=5-7)+4d^9nf\ (n=4-7)+4d^85snp\ (n=5-6)+4d^85snf\ (n=4-6)+4d^85pnd\ (n=5-6)+4d^84f5d$ for the even and odd parities, respectively.

Although they are not expected to be important in the present context, CP effects were introduced in the model. Core-valence correlation was considered within the framework of a CP potential and a correction to the dipole transition operator in a way described previously (see [22,23]). The estimate of these contributions requires the knowledge of the dipole polarizability of the ionic core, α_d, and of the cut-off radius, r_c. For the first parameter, we used the value computed by Fraga et al. [24] for the $[4s^24p^64d^8]$ Ru-like Xe^{10+} ion, i.e. $\alpha_d=0.61a_0^3$, while the cut-off radius, r_c, was chosen equal to $0.82a_0$ which corresponds to the HFR $\langle r\rangle$ value of the outermost core orbital 4d.

The HFR method has been combined with a least-squares optimization process of the radial parameters in order to reproduce as well as possible the experimental energy levels taken from Saloman [11] and Raineri et al. [13]. More precisely, for the $4d^{10}$, $4d^95s$, $4d^96s$, $4d^95d$ even configurations and for the $4d^95p$, $4d^95f$ odd configurations, all the average energies (E_{av}), spin–orbit parameters (ζ_{nl}) and monoconfiguration Slater integrals (F^k, G^k) were adjusted while, for $4d^96p$ and $4d^94f$, only the E_{av} and F^2 parameters were optimized. The average energy of $4d^97p$ was also adjusted. The standard deviations of the fits were found to be equal to $207\,cm^{-1}$ (even parity) and $164\,cm^{-1}$ (odd parity).

The HFR and HFR + CP lifetimes, as obtained in the present work, are reported in Table 1 (columns 4 and 5) for the energy levels belonging to the $4d^9 5p$, 5d, 6s, 6p and 5f configurations. As expected for such a highly ionized atom, the CP effects are not very important, the HFR+POL lifetimes being on average 9% longer than the HFR values.

Table 1
Calculated HFR, HFR + CP and MCDF lifetime values (in ns) of Xe IX and comparison with experimental results as obtained in the present work and also with the semiempirical results of [15].

Config.	Level[a]	E[a] (cm^{-1})	τ_{HFR}[b]	τ_{HFR+CP}[b]	τ_{MCDF}[b]	τ_{EXP}[c]	τ_{PREV}[d]
$4d^9 5p$	$^3P^0_2$	575 438	0.418	0.470	0.420	0.43 ± 0.04	0.300
$4d^9 5p$	$^3F^0_3$	578 986	0.420	0.467	0.439	0.43 ± 0.04	0.288
$4d^9 5p$	$^3F^0_2$	593 154	0.400	0.446	0.415		0.276
$4d^9 5p$	$^3P^0_1$	594 522	0.324	0.361	0.328		0.234
$4d^9 5p$	$^3F^0_4$	596 854	0.264	0.294	0.272	0.26 ± 0.03	0.183
$4d^9 5p$	$^1D^0_2$	602 541	0.272	0.301	0.271	0.46 ± 0.05	0.184
$4d^9 5p$	$^1P^0_1$	604 877	0.012	0.011	0.011		0.0121
$4d^9 5p$	$^3D^0_3$	605 410	0.243	0.268	0.244	0.25 ± 0.03	0.159
$4d^9 5p$	$^3P^0_2$	575 438	0.418	0.470	0.420	0.43 ± 0.04	0.300
$4d^9 5p$	$^3F^0_3$	578 986	0.420	0.467	0.439	0.43 ± 0.04	0.288
$4d^9 5p$	$^3F^0_2$	593 154	0.400	0.446	0.415		0.276
$4d^9 5p$	$^3P^0_1$	594 522	0.324	0.361	0.328		0.234
$4d^9 5p$	$^3F^0_4$	596 854	0.264	0.294	0.272	0.26 ± 0.03	0.183
$4d^9 5p$	$^1D^0_2$	602 541	0.272	0.301	0.271	0.46 ± 0.05	0.184
$4d^9 5p$	$^1P^0_1$	604 877	0.012	0.011	0.011		0.0121
$4d^9 5p$	$^3D^0_3$	605 410	0.243	0.268	0.244	0.25 ± 0.03	0.159
$4d^9 5p$	$^3P^0_0$	607 906	0.281	0.317	0.280		0.205
$4d^9 5p$	$^1F^0_3$	616 157	0.265	0.294	0.270	0.23 ± 0.02	0.181
$4d^9 5p$	$^3D^0_1$	618 269	0.046	0.044	0.048		0.0441
$4d^9 5p$	$^3D^0_2$	621 147	0.245	0.271	0.243		0.161
$4d^9 5d$	$^3S_1$	780 792	0.057	0.062	0.050		0.0480
$4d^9 5d$	$^3G_4$	788 522	0.055	0.058	0.046	0.077 ± 0.008	0.0434
$4d^9 5d$	$^3D_2$	790 022	0.054	0.058	0.047	0.050 ± 0.005	0.0427
$4d^9 5d$	$^3G_5$	790 742	0.065	0.070	0.053		0.0527
$4d^9 5d$	$^1P_1$	790 854	0.064	0.069	0.054		0.0525
$4d^9 5d$	$^3D_3$	792 488	0.056	0.060	0.047	0.055 ± 0.006	0.0436
$4d^9 5d$	$^1F_3$	795 332	0.065	0.069	0.052		0.0512
$4d^9 5d$	$^3P_2$	796 070	0.065	0.069	0.052		0.0510
$4d^9 5d$	$^3F_4$	797 063	0.066	0.071	0.053		0.0524
$4d^9 5d$	$^3P_0$	798 896	0.057	0.061	0.048		0.0453
$4d^9 5d$	$^3P_1$	803 860	0.060	0.063	0.051	0.080 ± 0.008	0.0486
$4d^9 5d$	$^3G_3$	805 240	0.055	0.058	0.046		0.0430
$4d^9 5d$	$^3D_1$	807 691	0.060	0.064	0.050		0.0482
$4d^9 5d$	$^1G_4$	809 314	0.066	0.071	0.053		0.0532
$4d^9 5d$	$^1D_2$	810 825	0.060	0.064	0.052		0.0457
$4d^9 5d$	$^3F_2$	811 675	0.061	0.064	0.048	0.036 ± 0.004	0.0483
$4d^9 5d$	$^3F_3$	813 696	0.066	0.070	0.053		0.0522
$4d^9 5d$	$^1S_0$	843 962	0.042	0.044	0.024		0.0287
$4d^9 6s$	$^3D_3$	901 686	0.030	0.028	0.031		
$4d^9 6s$	$^1D_2$	902 810	0.030	0.028	0.031		
$4d^9 6s$	$^3D_1$	918 346	0.030	0.028	0.031		
$4d^9 6s$	$^3D_2$	919 176	0.030	0.028	0.031		
$4d^9 6p$	$^3P^0_1$	963 320	0.023	0.028	0.038		
$4d^9 6p$	$^1P^0_1$	972 620	0.021	0.026	0.030		

[a] From NIST compilation [35] and Raineri et al. [13].
[b] This work: theoretical values (see the text).
[c] This work: experimental values obtained with the BFS technique.
[d] Previous work [15].

2.2. MCDF calculations

It is interesting to compare the results of the HFR calculations with those obtained with a completely independent theoretical method, i.e. the fully relativistic multiconfiguration Dirac–Fock approach (MCDF).

This is why we have also adopted this method in the present context. More precisely, we used the general-purpose relativistic atomic structure package (GRASP), originally developed by Grant and co-workers [25,26] and updated by Dyall et al. [27]. The computations were done with the extended average level (EAL) option, optimizing a weighted trace of the Hamiltonian using level weights proportional to $2J+1$. The orthogonality of the wavefunctions was consistently included in the differential equations by using off-diagonal Lagrange multipliers. The following non-relativistic configurations were considered in the vectorial basis: $4d^{10}+4d^{9}5s+4d^{9}6s+4d^{9}5d+4d^{8}5s^{2}+4d^{8}5p^{2}+4d^{8}5d^{2}+4d^{8}5s5d$ (even parity) and $4d^{9}5p+4d^{9}6p+4d^{9}4f+4d^{9}5f+4d^{8}5s5p+4d^{8}4f5s+4d^{8}5p5d$ (odd parity). This corresponds to 1260 relativistic configuration state functions. The calculations were completed with the inclusion of the relativistic two-body Breit interaction and of the quantum electrodynamics (QED) corrections due to self-energy (SE) and vacuum polarization (VP) using the routines developed by McKenzie et al. [28]. In these routines, the leading corrections to the Coulomb repulsion between electrons in QED are considered as a first-order perturbation using the transverse Breit operator [25], the second-order VP corrections are evaluated using the prescription of Fullerton and Rinker [29] and the SE contributions are estimated by interpolating the values obtained by Mohr [30,31] for 1s, 2s and 2p Coulomb orbitals. The nuclear effects were estimated by considering a uniform charge distribution in the nucleus with a xenon atomic weight equal to 131.29.

It was verified that the differences between computed and experimental levels in the $4d^{9}5s$, $4d^{9}6s$, $4d^{9}5d$, $4d^{9}5p$, $4d^{9}6p$ and $4d^{9}5f$ did not exceed 1–2% except for the $4d^{9}5f\ ^{1}P_{1}^{0}$ level for which a discrepancy of about 5% remained. It was also verified that for the most intense transitions, i.e. those most contributing to the radiative lifetimes, the MCDF *A*-values computed in the Babushkin gauge did not differ by more than 10–15% from those calculated in the Coulomb gauge.

The corresponding MCDF lifetime values are reported in Table 1 (column 6). It is interesting to observe that the MCDF and HFR results are in a very good agreement (within a few percent) indicating that the relativistic effects are adequately considered in the HFR model. As the HFR + CP calculation includes more correlation, we have decided to adopt the HFR-CP oscillator strengths and transition probabilities considering that they are the best ones obtained in the present paper.

The two sets of results obtained in the present work differ, however, systematically from the results obtained by Loginov [15]. In fact, for most of the levels, the latter lifetimes are systematically smaller indicating that some effects have not been adequately estimated in the semi-empirical calculations of [15]. These conclusions are confirmed by the fact that the results of [15] are also, in most cases, systematically lower than the experimental results (see the next section).

3. Experiment

The reliability of the present calculations was tested by comparisons to experimental results. So far, however, no experimental data have been published for this ion. For this reason, we have decided to perform lifetime measurements in Xe IX using the beam–foil method, one of the rare approaches able to provide experimental information on highly charged ions.

Beams of Xe^{+} ions have been produced by a 2 MV Van de Graaff accelerator equipped with a radio-frequency ion source filled with xenon gas. The beam was analyzed by a magnet and sent through a thin $20\,\mu g/cm^{2}$ home made carbon foil. The current intensity was kept below $\sim 1\,\mu A$ in order to increase the in-beam lifetime of the foil by avoiding its overheating.

The light produced by the beam–foil interaction was observed at right angle with a Seya-Namioka type spectrometer equipped with a 1 m radius 1200 l/mm concave grating coated with Pt for improved reflectivity in the UV. The wavelength resolution (FWMH) was of the order of ~0.1 nm (entrance slits width 50 μm). With this mounting, the efficiency of the grating was maximum around 60 nm. A small part of the spectrum registered around 66–78 nm is shown in Fig. 1.

The distance between the beam axis and the entrance slit, placed in the excitation chamber, was 15 mm and the width of the portion of ion beam (diameter 5 mm) viewed by the spectrometer was 0.06 mm, corresponding to a time window of ≈ 0.1 ns for a 1.9 MeV Xe beam. To measure the weak light signal, the exit slit was removed and replaced by a thin, back-illuminated, liquid nitrogen cooled CCD detector specially developed for far UV measurements. The CCD was tilted to an angle of 125° relatively to the spectrometer exit arm axis in order to be tangential to the Rowland circle. Under that geometry, it has a dispersion of 0.02 nm/pixel and detects light over a 20 nm wide region with a fairly constant resolution. The CCD detector system was supplied by the universities of Leicester and Lund. It is made of a EEV CCD15-11 chip of 27.6 × 6.9 mm (1040 × 280 of 27 × 27 μm square pixels) specially conditioned for UV light detection [32,33]. The CCD images were transferred to a networked computer and analyzed by a specially written software that eliminates the dark noise and filters the spikes due to gamma and X-rays. The XY image was transformed by binning the horizontal lines into a file containing a list of numbers representing the light intensity as a function of the wavelength. Xenon spectra were recorded in the wavelength region 35–110 nm at different ion beam energies in order to discriminate between ionization stages by studying the variation of intensity as a function of the ion speed [34]. The calibration of the spectra and the identification of the lines were based mainly on the recent compilation of Xe lines [11] available also on the NIST web site [35].

The light measurements were normalized to a fixed amount of charge entering the electrically isolated excitation chamber acting as a Faraday cup. The current was measured with a Ortec 439 current digitizer and the chamber was hold to

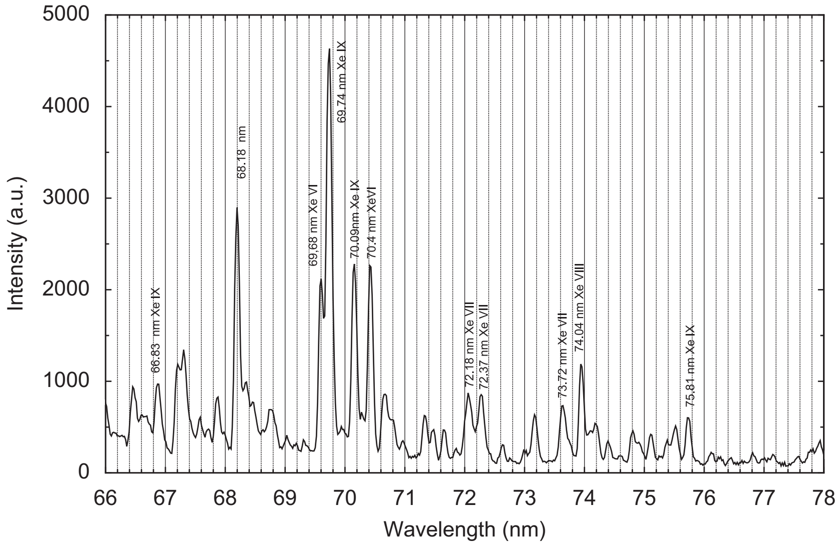

Fig. 1. Small region of the Xe beam–foil spectra obtained with a 1.9 MeV Xe^+ ion beam. A few transitions emitted by the ions Xe VI–Xe IX are indicated.

a potential of +90 V to reduce secondary electron loss through the chamber apertures. The whole system was working under vacuum (10^{-5} Torr).

Let us mention that the beam–foil excitation process produces spectra that are different from those of conventional hot plasma sources. In our spectra, some lines originating from $5p\,^1P_1^0$ (67.60 and 76.11 nm) and $5p\,^3D_1^0$ (61.99, 67.46, 69.07 nm) levels are missing or very weak whereas they are noted as strong or very strong in [9]. This can be explained by the fact that these two levels have a direct link to the Xe IX ground state ($4d^{10}\,^1S_0$), so that the population of these levels disappears very fastly to the ground state without any way to be repopulated by any post-foil excitation mechanism.

The decay curves have been obtained by moving the foil target upstream along the ion beam path. The recording of the line intensity as a function of the foil holder position along the beam axis was fully automatized [36] and the light intensity was normalized for each point to a constant beam charge crossing the foil. The displacement of the foil was measured with a resolution of 10 μm by a digital gauge (Mitutoyo 5 MQ65-5P). All the lifetime measurements were obtained with a 1.9 MeV Xe^+ beam, and a speed value of 1.60 mm/ns was used to convert all the distances to time (the energy loss inside the foil being deduced [37]).

To evaluate a line intensity at every position, the part of the CCD spectrum surrounding the line was fitted with a Gaussian in order to subtract the background and the amplitude of the Gaussian was used as a measurement of the line intensity. The decay data were fitted with a model describing the whole curve as a growing part (close to the foil) followed by a multi-exponential decay to take into account the possible cascading effect (see Fig. 2). The results presented in Table 1 are means of at least three measurements. The quoted error (10%) is larger than the variance of the measurements and covers possible systematic errors coming i.e. from a systematic error on the beam speed determination or some unaccounted cascading effects.

4. Results

Eleven lifetimes have been measured in the present work. The results are presented in column 7 of Table 1. Most of them agree quite well with the two sets of theoretical values (MCDF and HFR + CP) but disagree substantially from the semi-empirical results of [15].

The following comments concerning the measurements are relevant here:

- $5p\,^3P_2^0$ and $5p\,^3F_3^0$: The two lines at 81.947 nm ($5s\,^3D_2-5p\,^3F_3^0$) and 81.947 nm ($5s\,^3D_3-5p\,^3F_3^0$) are blended in our spectra and have comparable intensities. The mean lifetime deduced from the decay of the blended feature was 0.43 ns, very close to the predicted value for both levels.
- $5p\,^3F_4^0$: The lifetime of that level has been measured from the decay of the strong 69.742 nm line ($5s\,^3D_3-5p\,^3F_4^0$). It has not been possible to measure the third level (i.e. $^3F_2^0$).
- $5p\,^1D_2^0$: The measurement from the line at 68.688 nm ($5s\,^1D_2-5p\,^1D_2^0$) is substantially larger than all the calculated results. There is no clear explanation for the discrepancy.

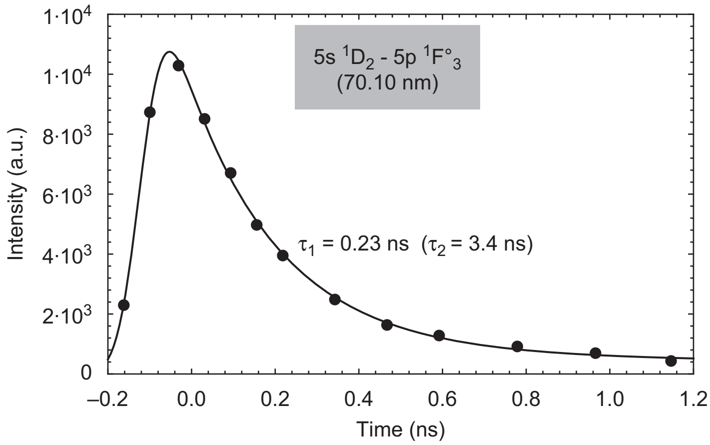

Fig. 2. Decay curve of the Xe IX $5p\,^1F_3^0$ level. The $5s\,^1D_2-5p\,^1F_3^0$ transition has been used for obtaining this curve.

Table 2
Calculated oscillator strengths (log *gf*) and transition probabilities (*gA*) in Xe IX.

λ^a (nm)	Low. level[b]				Upp. level[b]				log *gf*[c]	*gA*[c] (s^{-1})
	E (cm^{-1})	Conf.	Term	*J*	*E* (cm^{-1})	Conf.	Term	*J*		
16.1742	0	$4d^{10}$	^1S	0	618 269	$4d^95p$	$^3D^0$	1	−0.65	5.67E + 10
16.5323	0	$4d^{10}$	^1S	0	604 877	$4d^95p$	$^1P^0$	1	0.04	2.68E + 11
30.6520	575 438	$4d^95p$	$^3P^0$	2	901 686	$4d^96s$	^3D	3	−0.04	6.53E + 10
30.6728*	593 154	$4d^95p$	$^3F^0$	2	919 176	$4d^96s$	^3D	2	−0.48	2.34E + 10
30.7500	593 154	$4d^95p$	$^3F^0$	2	918 346	$4d^96s$	^3D	1	−0.27	3.76E + 10
30.8020	594 522	$4d^95p$	$^3P^0$	1	919 176	$4d^96s$	^3D	2	−0.47	2.36E + 10
30.8800	578 986	$4d^95p$	$^3F^0$	3	902 810	$4d^96s$	^1D	2	−0.06	6.15E + 10
30.9880	578 986	$4d^95p$	$^3F^0$	3	901 686	$4d^96s$	^3D	3	−0.32	3.33E + 10
31.8150	604 877	$4d^95p$	$^1P^0$	1	919 176	$4d^96s$	^3D	2	−0.66	1.44E + 10
32.2100	607 906	$4d^95p$	$^3P^0$	0	918 346	$4d^96s$	^3D	1	−0.74	1.18E + 10
32.2939*	593 154	$4d^95p$	$^3F^0$	2	902 810	$4d^96s$	^1D	2	−0.98	6.66E + 09
32.4380	594 522	$4d^95p$	$^3P^0$	1	902 810	$4d^96s$	^1D	2	−0.63	1.48E + 10
32.8040	596 854	$4d^95p$	$^3F^0$	4	901 686	$4d^96s$	^3D	3	0.21	1.01E + 11
33.0030	616 157	$4d^95p$	$^1F^0$	3	919 176	$4d^96s$	^3D	2	0.10	7.63E + 10
33.3050	602 541	$4d^95p$	$^1D^0$	2	902 810	$4d^96s$	^1D	2	−0.10	4.76E + 10
33.3270	618 269	$4d^95p$	$^3D^0$	1	918 346	$4d^96s$	^3D	1	−0.34	2.75E + 10
33.5530	621 147	$4d^95p$	$^3D^0$	2	919 176	$4d^96s$	^3D	2	−0.24	3.42E + 10
33.5646*	604 877	$4d^95p$	$^1P^0$	1	902 810	$4d^96s$	^1D	2	−0.58	1.57E + 10
33.6240	605 410	$4d^95p$	$^3D^0$	3	902 810	$4d^96s$	^1D	2	−0.36	2.57E + 10
33.6510	621 147	$4d^95p$	$^3D^0$	2	918 346	$4d^96s$	^3D	1	−0.48	1.95E + 10
33.7530	605 410	$4d^95p$	$^3D^0$	3	901 686	$4d^96s$	^3D	3	−0.09	4.79E + 10
41.8257	604 877	$4d^95p$	$^1P^0$	1	843 962	$4d^95d$	^1S	0	−0.31	1.87E + 10
45.7624	593 154	$4d^95p$	$^3F^0$	2	811 675	$4d^95d$	^3F	2	−0.27	1.71E + 10
45.9407	593 154	$4d^95p$	$^3F^0$	2	810 825	$4d^95d$	^1D	2	−0.40	1.27E + 10
46.0719	575 438	$4d^95p$	$^3P^0$	2	792 488	$4d^95d$	^3D	3	0.08	3.76E + 10
46.2229	578 986	$4d^95p$	$^3F^0$	3	795 332	$4d^95d$	^1F	3	−0.48	1.03E + 10
46.2319	594 522	$4d^95p$	$^3P^0$	1	810 825	$4d^95d$	^1D	2	−0.32	1.51E + 10
46.4190	575 438	$4d^95p$	$^3P^0$	2	790 854	$4d^95d$	^1P	1	−0.51	9.48E + 09
46.6010	575 438	$4d^95p$	$^3P^0$	2	790 022	$4d^95d$	^3D	2	0.26	5.58E + 10
46.8386	578 986	$4d^95p$	$^3F^0$	3	792 488	$4d^95d$	^3D	3	0.12	4.03E + 10
46.9100	594 522	$4d^95p$	$^3P^0$	1	807 691	$4d^95d$	^3D	1	−0.86	4.18E + 09
47.1498	593 154	$4d^95p$	$^3F^0$	2	805 240	$4d^95d$	^3G	3	0.42	7.79E + 10
47.3864	578 986	$4d^95p$	$^3F^0$	3	790 022	$4d^95d$	^3D	2	−0.42	1.12E + 10

Table 2 (*continued*)

λ^a (nm)	Low. level[b]				Upp. level[b]				$\log gf^c$	gA^c (s^{-1})
	E (cm^{-1})	Conf.	Term	J	E (cm^{-1})	Conf.	Term	J		
47.7240	578 986	$4d^95p$	$^3F^0$	3	788 522	$4d^95d$	^3G	4	0.65	1.31E+11
47.7685	594 522	$4d^95p$	$^3P^0$	1	803 860	$4d^95d$	^3P	1	−0.25	1.65E+10
48.008	602 541	$4d^95p$	$^1D^0$	2	810 825	$4d^95d$	^1D	2	−0.99	2.95E+09
48.3556	604 877	$4d^95p$	$^1P^0$	1	811 675	$4d^95d$	^3F	2	−0.45	1.00E+10
48.5560	604 877	$4d^95p$	$^1P^0$	1	810 825	$4d^95d$	^1D	2	−0.49	9.16E+09
48.6959	575 438	$4d^95p$	$^3P^0$	2	780 792	$4d^95d$	^3S	1	0.12	3.66E+10
48.9300	594 522	$4d^95p$	$^3P^0$	1	798 896	$4d^95d$	^3P	0	−0.28	1.48E+10
49.2817	593 154	$4d^95p$	$^3F^0$	2	796 070	$4d^95d$	^3P	2	−0.77	4.63E+09
49.3063*	604 877	$4d^95p$	$^1P^0$	1	807 691	$4d^95d$	^3D	1	−0.66	6.01E+09
49.3343	602 541	$4d^95p$	$^1D^0$	2	805 240	$4d^95d$	^3G	3	−0.08	2.28E+10
49.4614	593 154	$4d^95p$	$^3F^0$	2	795 332	$4d^95d$	^1F	3	−0.16	1.90E+10
49.6162	594 522	$4d^95p$	$^3P^0$	1	796 070	$4d^95d$	^3P	2	−0.35	1.22E+10
49.9478	596 854	$4d^95p$	$^3F^0$	4	797 063	$4d^95d$	^3F	4	0.12	3.52E+10
50.0532	607 906	$4d^95p$	$^3P^0$	0	807 691	$4d^95d$	^3D	1	−0.13	1.99E+10
50.2566	604 877	$4d^95p$	$^1P^0$	1	803 860	$4d^95d$	^3P	1	−0.49	8.60E+09
50.6230	616 157	$4d^95p$	$^1F^0$	3	813 696	$4d^95d$	^3F	3	−0.06	2.28E+10
50.9332	594 522	$4d^95p$	$^3P^0$	1	790 854	$4d^95d$	^1P	1	−0.41	1.00E+10
51.1159	596 854	$4d^95p$	$^3F^0$	4	792 488	$4d^95d$	^3D	3	−0.52	7.66E+09
51.3695*	616 157	$4d^95p$	$^1F^0$	3	810 825	$4d^95d$	^1D	2	−0.75	4.50E+09
51.5762	596 854	$4d^95p$	$^3F^0$	4	790 742	$4d^95d$	^3G	5	0.77	1.45E+11
51.6714	602 541	$4d^95p$	$^1D^0$	2	796 070	$4d^95d$	^3P	2	0.12	3.30E+10
51.7050	618 269	$4d^95p$	$^3D^0$	1	811 675	$4d^95d$	^3F	2	0.21	4.04E+10
51.7714	616 157	$4d^95p$	$^1F^0$	3	809 314	$4d^95d$	^1G	4	0.67	1.17E+11
51.8700	602 541	$4d^95p$	$^1D^0$	2	795 332	$4d^95d$	^1F	3	0.23	4.16E+10
51.9329*	618 269	$4d^95p$	$^3D^0$	1	810 825	$4d^95d$	^1D	2	−0.82	3.76E+09
51.9347	621 147	$4d^95p$	$^3D^0$	2	813 696	$4d^95d$	^3F	3	0.43	6.71E+10
52.1730	596 854	$4d^95p$	$^3F^0$	4	788 522	$4d^95d$	^3G	4	−0.44	8.86E+09
52.1783	605 410	$4d^95p$	$^3D^0$	3	797 063	$4d^95d$	^3F	4	0.53	8.26E+10
52.3037	604 877	$4d^95p$	$^1P^0$	1	796 070	$4d^95d$	^3P	2	−0.38	1.03E+10
52.4494*,†	605 410	$4d^95p$	$^3D^0$	3	796 070	$4d^95d$	^3P	2	−1.00	2.45E+09
52.4857*,†	621 147	$4d^95p$	$^3D^0$	2	811 675	$4d^95d$	^3F	2	−0.87	3.25E+09
52.6523	605 410	$4d^95p$	$^3D^0$	3	795 332	$4d^95d$	^1F	3	−0.03	2.24E+10
52.7206	621 147	$4d^95p$	$^3D^0$	2	810 825	$4d^95d$	^1D	2	0.02	2.53E+10
52.7929	618 269	$4d^95p$	$^3D^0$	1	807 691	$4d^95d$	^3D	1	−0.38	9.95E+09
52.8876	616 157	$4d^95p$	$^1F^0$	3	805 240	$4d^95d$	^3G	3	−0.59	6.16E+09
53.1040	602 541	$4d^95p$	$^1D^0$	2	790 854	$4d^95d$	^1P	1	−0.62	5.73E+09
53.4528	605 410	$4d^95p$	$^3D^0$	3	792 488	$4d^95d$	^3D	3	−0.04	2.14E+10
53.6855*	594 522	$4d^95p$	$^3P^0$	1	780 792	$4d^95d$	^3S	1	−0.82	3.49E+09
53.7701	604 877	$4d^95p$	$^1P^0$	1	790 854	$4d^95d$	^1P	1	−0.23	1.37E+10
53.8820	618 269	$4d^95p$	$^3D^0$	1	803 860	$4d^95d$	^3P	1	−0.59	5.91E+09
54.1665	605 410	$4d^95p$	$^3D^0$	3	790 022	$4d^95d$	^3D	2	−0.27	1.22E+10
54.3204*	621 147	$4d^95p$	$^3D^0$	2	805 240	$4d^95d$	^3G	3	−0.76	3.89E+09
54.6118	605 410	$4d^95p$	$^3D^0$	3	788 522	$4d^95d$	^3G	4	−0.63	5.29E+09
54.7309	621 147	$4d^95p$	$^3D^0$	2	803 860	$4d^95d$	^3P	1	−0.54	6.41E+09
56.1013	602 541	$4d^95p$	$^1D^0$	2	780 792	$4d^95d$	^3S	1	−0.82	3.25E+09
65.8146	453 468	$4d^95s$	^3D	3	605 410	$4d^95p$	$^3D^0$	3	0.04	1.70E+10
66.1812	470 048	$4d^95s$	^3D	1	621 147	$4d^95p$	$^3D^0$	2	−0.33	7.16E+09
67.3602	456 956	$4d^95s$	^3D	2	605 410	$4d^95p$	$^3D^0$	3	−0.25	8.23E+09
67.4673	470 048	$4d^95s$	^3D	1	618 269	$4d^95p$	$^3D^0$	1	−0.21	9.06E+09
67.6040	456 956	$4d^95s$	^3D	2	604 877	$4d^95p$	$^1P^0$	1	−0.56	4.03E+09
67.7280	473 496	$4d^95s$	^1D	2	621 147	$4d^95p$	$^3D^0$	2	−0.13	1.07E+10
68.6885	456 956	$4d^95s$	^3D	2	602 541	$4d^95p$	$^1D^0$	2	−0.03	1.34E+10
69.7417	453 468	$4d^95s$	^3D	3	596 854	$4d^95p$	$^3F^0$	4	0.35	3.06E+10
70.0962	473 496	$4d^95s$	^1D	2	616 157	$4d^95p$	$^1F^0$	3	0.21	2.22E+10

Table 2 (*continued*)

λ^a (nm)	Low. level[b]				Upp. level[b]				log gf^c	gA^c (s^{-1})
	E (cm^{-1})	Conf.	Term	J	E (cm^{-1})	Conf.	Term	J		
72.5378	470 048	$4d^95s$	^3D	1	607 906	$4d^95p$	$^3P^0$	0	−0.61	3.15E+09
72.6923	456 956	$4d^95s$	^3D	2	594 522	$4d^95p$	$^3P^0$	1	−0.38	5.27E+09
73.4224	456 956	$4d^95s$	^3D	2	593 154	$4d^95p$	$^3F^0$	2	−0.69	2.55E+09
74.1683	470 048	$4d^95s$	^3D	1	604 877	$4d^95p$	$^1P^0$	1	−0.95	1.37E+09
76.1125	473 496	$4d^95s$	^1D	2	604 877	$4d^95p$	$^1P^0$	1	−0.48	3.81E+09
77.4916	473 496	$4d^95s$	^1D	2	602 541	$4d^95p$	$^1D^0$	2	−0.92	1.34E+09
79.6712	453 468	$4d^95s$	^3D	3	578 986	$4d^95p$	$^3F^0$	3	−0.29	5.37E+09
81.2297	470 048	$4d^95s$	^3D	1	593 154	$4d^95p$	$^3F^0$	2	−0.23	6.00E+09
81.9470	456 956	$4d^95s$	^3D	2	578 986	$4d^95p$	$^3F^0$	3	−0.02	9.56E+09
81.9875	453 468	$4d^95s$	^3D	3	575 438	$4d^95p$	$^3P^0$	2	0.01	1.02E+10
82.6270	473 496	$4d^95s$	^1D	2	594 522	$4d^95p$	$^3P^0$	1	−0.57	2.66E+09
83.5729	473 496	$4d^95s$	^1D	2	593 154	$4d^95p$	$^3F^0$	2	−0.56	2.62E+09

*Starred wavelengths have not been observed. They have been derived from experimental energy levels. †Those two lines have been observed in [12], but not listed in [11]. Only the transitions $4d^{10}-4d^95p$, $4d^95p-4d^96s$, $4d^95p-4d^95d$ and $4d^95s-4d^95p$ emitted from levels with $E<950\,000\,cm^{-1}$ and for which log $gf \geqslant -1$ are listed.

[a] From the compilation by Saloman [11] and Raineri et al. [13].

[b] From the compilation by Saloman [11] and Raineri et al. [13].

[c] HFR + CP calculations (this work).

- 5p $^3D^0_3$: The experimental result has been obtained from the transition at 75.81 nm (5s $^1D_2$–5p $^3D^0_3$). Even if it is an intercombination line, its intensity was strong enough for decay recording. The lifetime value obtained, 0.25 ns, is in close agreement with the theoretical lifetimes (HFR and MCDF).
- 5p $^1F^0_3$: For this level also, experiment and theory agree quite well. The wavelength considered for the measurement appears in our spectra as a very strong line located at 70.092 nm (5s $^1D_2$−5p $^1F^0_3$).
- 5d $^3G_4$: The lifetime (0.077 ns) has been deduced from the decay of the 47.724 nm (5p $^3F^0_3$−5d $^3G_4$) transition and is larger than the theoretical predictions.
- 5d $^3D_2$: The short lifetime of 0.05 ns has been measured from the decay analysis of the 46.6 nm line (5p $^3D^0_2$−5d $^3D_2$) and is in agreement with theory.
- 5d $^3D_3$: The signal obtained for this level, by observing the 46.072 nm (5p $^3P^0_2$−5d $^3D_3$) was good and the experimental result is expected to be accurate. It does agree quite well with the theoretical values. It is also close to the lifetime value measured for the $^3D_2$ level.
- 5d $^3P_1$: The experimental lifetime was obtained from the wavelength at 53.882 nm (5p $^3D^0_1$ − 5d $^3P_1$) and is slightly longer than the theoretical predictions.
- 5d $^3F_2$: The experimental lifetime obtained for this level from the 45.762 nm weak line (5p $^3F^0_2$−5d $^3F_2$) is lower than all the theoretical values including that of [15].

In view of the overall agreement theory-experiment giving some weight to the theoretical models used in the present paper, we propose in Table 2 a detailed set of weighted oscillator strengths (log gf) and transition probabilities (gA) in Xe IX. Only the transitions $4d^{10}-4d^95p$, $4d^95p-4d^96s$, $4d^95p-4d^95d$ and $4d^95s-4d^95p$ emitted from levels with $E<950\,000\,cm^{-1}$ and for which log $gf \geqslant -1$ are listed. For most of the transitions quoted, the accuracy is expected to be within 10–15%.

5. Conclusions

Transition probabilities are presented for a set of 99 $4d^{10} - 4d^95p$, $4d^95s-4d^95p$, $4d^95p-4d^95d$ and $4d^95p-4d^96s$ transitions of Xe IX in the wavelength range between 16 and 84 nm. They have been obtained with a HFR method including CP effects. The accuracy of the results has been assessed through comparisons of this approach with a completely independent theoretical method (i.e. the MCDF method) but also through a comparison with experimental results obtained by the beam–foil technique for 11 levels belonging to the $4d^95p$ and $4d^95d$ configurations.

Acknowledgements

We are indebted to the Institut Universitaire des Sciences Nucléaires for its financial support. The technical help of M. Clar (IPNAS, U.Lg., Liège, Belgium) is gratefully acknowledged. Financial support from the Belgian F.R.S.-FNRS is acknowledged by two of us (E.B. and P.Q.) who are, respectively, Research Director and Senior Research Associate of this organization. One of us (S.E.Y.) has received a grant from the Belgian DGCD through the project PIC-MAC-1245 and a partial support from the ICTP through the OEA-AC-71.

References

[1] Péquignot D, Baluteau J-P. The discovery of heavy elements ($Z>30$) in NGC7027. Astron Astrophys 1994;283:593–625.
[2] Butler K, Schöning T. Effective collision strengths for electron impact excitation of Xe III, Xe IV, Xe VI and Ba II, Ba IV. Astron Astrophys Suppl 1998;128:581–8.
[3] Zhang Y, Williams R, Pellegrini E, Cavagnolo K, Baldwin JA, Sharpee B, et al. s-Process abundances in planetary nebulae: Br, Kr and Xe. Planetary Nebulae in our galaxy and beyond. In: Barlow MJ, Mendez RH, editors, Proceedings of the IAU Symposium, vol. 234, 2006.
[4] Lemoff BE, Yin GY, Gordon III CL, Barty CPJ, Harris SE. Demonstration of a 10-Hz femtosecond-pulse-driven XUV laser at 41.8 nm in Xe IX. Phys Rev Lett 1995;74:1574–7.
[5] Lemoff BE, Yin GY, Gordon III CL, Barty CPJ, Harris SE. Femtosecond-pulse-driven 10-Hz 41.8-nm laser in Xe IX. Phys Rev Lett 1995;74:1574–7;
Lemoff BE, Yin GY, Gordon III CL, Barty CPJ, Harris SE. Femtosecond-pulse-driven 10-Hz 41.8-nm laser in Xe IX. J Opt Soc Am 1996;B13:180–4.
[6] Fahy K, Sokell E, O'Sullivan G, Aguilar A, Pomeroy JM, Tan JN, et al. Extreme-ultraviolet spectroscopy of highly charged xenon ions created using an electron-beam ion trap. Phys Rev A 2007;75:032520.
[7] Sugar J, Kaufman V. Resonance lines in the Pd I isoelectronic sequence: I VIII to Ho XXII. Phys Scr 1982;26:419–21.
[8] van Kampen P, Hallin R, Heijkenskjöld F, Langereis A, Larsson MO, Nordling C, et al. Wavelengths and energy levels of the 4d95s–4d95p transition array of Xe IX. Phys Scr 1994;49:198–200.
[9] Churilov SS, Ryabtsev AN, Tchang-Brillet W-ÜL, Wyart J-F. Analysis of the Spectra of Pd-like Ions from Xe IX Through Ce XIII. Phys Scr 2002;66: 293–307.
[10] Churilov SS, Joshi YN. Revised and extended analysis of six times ionized xenon: Xe VII. Phys Scr 2002;65:40–5.
[11] Saloman EB. Energy levels and observed spectral lines of xenon, Xe I through Xe LIV. J Phys Chem Ref Data 2004;33:765–921.
[12] Callegari F, Gallardo M, Raineri M, Trigueros AG, Reyna Almandos JG. Spectral analysis of the 4d95d and 4d95f configurations in octuple ionization of xenon, XeIX. JQSRT 2002;73:13–22.
[13] Raineri M, Gallardo M, Reyna Almandos JG. Spectral analysis of the 4d96s configuration in eight times ionized xenon, Xe IX. JQSRT 2006;102:391–5.
[14] Younger SM. Theoretical line strengths for the 4d101S–4d94f1Po resonance transition in the palladium isoelectronic sequence. Phys Rev A 1980;22:2682–9.
[15] Loginov AV. Palladium-like XeIXCeXIII spectra: effective interaction and radiative constants. Opt Spectrosc 2003;95(6):869–72.
[16] Safronova UI, Cowan TE, Johnson WR. Relativistic many-body calculations of excitation energies, line strengths, transition rates, and oscillator strengths in Pd-like ions. Can J Phys 2005;83:813–28.
[17] Safronova UI, Bista R, Bruch R, Merabet H. Relativistic many-body calculations of atomic properties in Pd-like ions. Can J Phys 2008;86:131–49.
[18] Biémont É, Quinet P, Zeippen CJ. Transition Probabilities in Xe V. Phys Scr 2005;71:163–9.
[19] Biémont É, Buchard V, Garnir H-P, Lefèbvre P-H, Quinet P. Radiative lifetime and oscillator strength determinations in Xe VI. Eur Phys J D 2005;33:181–91.
[20] Biémont É, Clar M, Fivet V, Garnir H-P, Palmeri P, Quinet P, et al. Lifetime and transition probability determination in xenon ions—the cases of Xe VII and Xe VIII. Eur Phys J D 2007;44:23–33.
[21] Cowan RD. The theory of atomic structure and spectra. Berkeley: University of California Press; 1981.
[22] Biémont É, Quinet P. Recent advances in the study of lanthanide atoms and ions. Phys Scr T 2003;105:38–54.
[23] Quinet P, Palmeri P, Biémont E, McCurdy MM, Rieger G, Pinnington EH, et al. Experimental and theoretical radiative lifetimes, branching fractions and oscillator strengths in Lu II. Mon Not Roy Astron Soc 1999;307:934–40.
[24] Fraga S, Karwowski J, Saxena KMS. Handbook of atomic data. Amsterdam: Elsevier; 1976.
[25] Grant IP, McKenzie BJ. J Phys B 1980;13:2671–81.
[26] Grant IP, McKenzie BJ, Norrington PH, Mayers DF, Pyper NC. The transverse electron–electron interaction in atomic structure calculations. Comput Phys Commun 1980;21:207–31.
[27] Dyall KG, Grant IP, Johnson CT, Parpia FA, Plummer EP. An atomic multiconfigurational Dirac–Fock package. Comput Phys Commun 1989;55:425–56.
[28] McKenzie BJ, Grant IP, Norrington PH. A program to calculate transverse Breit and QED corrections to energy levels in a multiconfiguration Dirac–Fock environment. Comput Phys Commun 1980;21:233–46.
[29] Fullerton LW, Rinker GA. Accurate and efficient methods for the evaluation of vacuum-polarization potentials of order Z^{α} and Z^{α^2}. Phys Rev A 1976; 13:1283–7.
[30] Mohr PJ. Numerical evaluation of the $^1S_{1/2}$-state radiative level shift. Ann Phys 1974;88:52–87.
[31] Mohr PJ. Lamb shift in a strong Coulomb potential. Phys Rev Lett 1975;34:1050–2.
[32] Hutton R, Zou Y, Hult S, Martinson I, Ando K, Nyström B, et al. A CCD Detector system for beam–foil spectroscopy. Phys Scr T 1999;80B:532–3.
[33] Garnir H-P, Lefébvre P-H. Quantum efficiency of back-illuminated CCD detectors in the VUV region (30–200 nm). Nucl. Instrum. Method B 2005;235:530–4.
[34] Garnir HP. Energy dependence of Xe ion lines produced by beam–foil interaction. In: Proceedings of ASOS9 meeting. J Phys Conf Ser, 2008, in press.
[35] ⟨http://physics.nist.gov/PhysRefData/ASD/index.html⟩.
[36] Monjoie FS, Garnir HP. The University of Liège user interface for laboratory experiment control. Comput Phys Commun 1990;61:267–73.
[37] Garnir-Monjoie FS, Baudinet-Robinet Y, Garnir HP, Dumont PD. Empirical relation for electronic stopping power of heavy ions in carbon. J Phys 1980;41:599–601.